

## Core-shell-structured bimetallic clusters and nanowires

This article has been downloaded from IOPscience. Please scroll down to see the full text article.

2007 J. Phys.: Condens. Matter 19 356217

(<http://iopscience.iop.org/0953-8984/19/35/356217>)

View [the table of contents for this issue](#), or go to the [journal homepage](#) for more

Download details:

IP Address: 129.252.86.83

The article was downloaded on 29/05/2010 at 04:34

Please note that [terms and conditions apply](#).

# Core-shell-structured bimetallic clusters and nanowires

Daojian Cheng, Wenchuan Wang<sup>1</sup> and Shiping Huang

Division of Molecular and Materials Simulation, Key Lab for Nanomaterials, Ministry of Education, Beijing University of Chemical Technology, Beijing 100029, People's Republic of China

E-mail: wangwc@mail.buct.edu.cn

Received 20 March 2007, in final form 12 June 2007

Published 20 August 2007

Online at [stacks.iop.org/JPhysCM/19/356217](http://stacks.iop.org/JPhysCM/19/356217)

## Abstract

We report the structures of Ag–Cu and Ag–Ni bimetallic clusters and nanowires (NWs), which are well known as effective Ag-based catalysts, by using an effective semi-grand-canonical ensemble Monte Carlo method. The metal–metal interactions are modeled by the second-moment approximation of the tight-binding potentials. The simulation results show that the Ag–Cu and Ag–Ni bimetallic nanomaterials, including clusters and NWs, possess core–shell structures at different compositions, in which the Ag atoms lie on the surface, while the Cu or Ni atoms occupy the cores of the clusters and NWs. It is found that the pentagonal multi-shell-type structure can be transformed into cylindrical multi-shell-type structures for Ag–Cu and Ag–Ni bimetallic NWs at 100, 300, and 500 K. On the other hand, with the increase of Ag mole fraction in the Ag–Cu and Ag–Ni bimetallic clusters, the Ag atoms occupy the surface shell first, then the interior shell, and finally the central sites of the clusters. It is also found that the initial shape, composition, and temperature have little effect on the core–shell structures of the bimetallic clusters and NWs. The formation of core–shell Ag–Cu and Ag–Ni bimetallic clusters and NWs is due to the fact that a single Ag impurity is favorable to be situated in the core of the Cu or Ni clusters and NWs.

(Some figures in this article are in colour only in the electronic version)

## 1. Introduction

In recent years considerable experimental and theoretical efforts have been put into nanomaterials due to their dramatically different behavior from that of bulk materials. Bimetallic nanomaterials are more promising for catalytic, optical, and magnetic applications

<sup>1</sup> Author to whom any correspondence should be addressed.

than monometallic ones [1–11]. One such nanomaterial is the bimetallic cluster. Besides their peculiar properties devoted to industrial applications, bimetallic clusters are interesting since their properties depend not only on size but also on composition and atomic ordering [12, 13]. For example, it was observed that the Pd–Pt clusters with a Pd content of 80% are the most active catalyst, and in those clusters the Pt atoms are fully covered by Pd atoms [2, 14]. This strongly suggests that the composition and atomic ordering have a significant effect on the catalytic activity of the bimetallic clusters. Another nanomaterial is the bimetallic nanowire (NW). Studies of bimetallic nanowires have attracted much attention because of their small size, magic structure, and composition effect [15, 16].

Considerable experimental efforts have been focused on the preparations and properties of bimetallic nanomaterials. For example, bimetallic clusters have been prepared extensively by co-reduction and successive reduction of two metal salts, and they can be characterized by different experimental techniques, such as extended x-ray absorption fine structure (EXAFS), infrared (IR) spectroscopy, and transmission electron microscopy (TEM) [2]. Also, bimetallic NWs have been fabricated extensively by direct electrodeposition into the pores of a host template. For example, Li *et al* [17, 18] fabricated highly ordered Co–Pt NW arrays by direct electrodeposition into the pores of a porous anodic aluminum oxide (AAO) template. Liu *et al* [19] prepared Fe–Ni NW alloys by electrodepositing  $\text{Fe}^{2+}$  and  $\text{Ni}^{2+}$  into a porous alumina template (PAT). Choi and Woo [11] synthesized a Pt–Ru NW network in a kind of meso-molecular sieve SBA-15 template, and found that the Pt–Ru NW used as an anode material in a direct methanol fuel cell (DMFC) shows higher performance than that with Pt–Ru black.

Structural models are very important for understanding the catalytic, optical, and magnetic properties of bimetallic clusters and NWs. The core–shell structure is one such model; it was found in bimetallic clusters by using experimental [20–22] and theoretical methods [23–27]. Rossi *et al* [25, 28, 29] reported the genetic algorithm global optimization method for a wide range of bimetallic clusters, Ag–Cu, Ag–Ni, Cu–Au, Ag–Au, Ag–Pd, and Pd–Pt, with a size of 34 and 38 atoms and different compositions, and found that those systems possess core–shell structures. Ferrando and co-workers [23, 30–32] studied Ag–Cu, Ag–Ni, and Ag–Pd bimetallic clusters by molecular dynamics simulations, and found core–shell structures in the systems. Mariscal *et al* [33] used collision as a new way, based on molecular dynamics simulations, to obtain the core–shell Pt–Au bimetallic clusters. In contrast, there are only a few reports of the study of the core–shell structures of bimetallic NWs. Wang *et al* [15] studied the geometrical and magnetic properties of core–shell Cu–Co bimetallic NWs by using empirical genetic algorithm simulations.

In this work, our attention is given to Ag–Cu and Ag–Ni nanomaterials, including clusters and NWs. The main reason for choosing Ag–Cu and Ag–Ni systems is that they are very effective Ag-based catalysts [10, 34–37], and they have been prepared and characterized by using experimental methods. The theoretical studies mentioned above have revealed some detailed structures of Ag–Cu and Ag–Ni bimetallic clusters. However, only small sizes of 34 and 38 atoms were studied for Ag–Cu and Ag–Ni bimetallic clusters by using the genetic algorithm global optimization method [28], due to the limitation of computational expenses. Also, by using molecular dynamics simulations [23, 32], only core–shell structures with single-layer Ag shells and some fixed compositions can be obtained for Ag–Cu and Ag–Ni bimetallic clusters. Thus, there is a need to study Ag–Cu and Ag–Ni bimetallic clusters with larger sizes and all compositions. In addition, little attention has been paid to the detailed structures of Ag–Cu and Ag–Ni bimetallic NWs.

In this paper, we present an effective Monte Carlo method to obtain the ground-state structures of bimetallic clusters and NWs for Ag–Cu and Ag–Ni with larger sizes and different compositions. We apply this method to study the structures of four systems, i.e. Ag–Cu

bimetallic clusters and NWs, and Ag–Ni bimetallic clusters and NWs. We use the second-moment approximation of the tight-binding potentials for the metal–metal interactions. The effects of initial shape, composition, and temperature on the structures of Ag–Cu and Ag–Ni bimetallic clusters and NWs are addressed. In section 2, we discuss the energetic model and the computational methods. In section 3, results and discussion of Ag–Cu and Ag–Ni bimetallic nanomaterials, including clusters and NWs, are presented. In section 4, we give the conclusions of this work.

## 2. Computational details

### 2.1. Initial cluster and nanowire configurations

In this work we used the icosahedral (Ico-type) and decahedral (Dec-type) shapes to model the initial Ag–Cu and Ag–Ni bimetallic clusters, and the initial clusters of interest contain 147 and 309 atoms. To describe multi-shell-type NWs, we use the notation  $n$ – $n_1$ – $n_2$ – $n_3$ , which was derived by Kondo and Takayanagi [38]. An  $n$ – $n_1$ – $n_2$ – $n_3$  NW consists of coaxial tubes with  $n$ ,  $n_1$ ,  $n_2$ ,  $n_3$  helical atom rows from outer tube to inner tube ( $n > n_1 > n_2 > n_3$ ). The Ag–Cu and Ag–Ni bimetallic NWs of interest possess the 15–10–5–1 and 10–5–1 pentagonal multi-shell-type (PMS-type) structure [39], which is composed of a central atomic strand and pentangular tubes made of five-times-folded  $\langle 100 \rangle$  sheets. Details of the initial shapes here are shown in figure 1.

### 2.2. The TB-SMA potential

The atom–atom interactions are modeled by the second-moment approximation of the tight-binding (TB-SMA) potentials, which has been widely used to study the structures of metal clusters [23–25, 28–30, 32] and NWs [15, 39–42]. Within the TB-SMA potential [43], the total energy of a system is calculated as

$$E_{\text{total}} = \sum_i (E_{\text{R}}^i + E_{\text{B}}^i) \quad (1)$$

where  $E_{\text{R}}^i$  and  $E_{\text{B}}^i$  are the Born–Mayer ion–ion repulsion and band terms, respectively. Both terms can be written for an atom  $i$  as

$$E_{\text{R}}^i = \sum_j A e^{-p(r_{ij}/r_0-1)}, \quad (2)$$

$$E_{\text{B}}^i = - \left\{ \sum_j \xi^2 e^{-2q(r_{ij}/r_0-1)} \right\}^{1/2}, \quad (3)$$

where  $r_{ij}$  is the distance between atoms  $i$  and  $j$  in the cluster.  $r_0$  is the nearest-neighbor distance in the pure metals (Ag, Cu and Ni), and is taken as the average of the pure ones for the heterometallic interactions (Ag–Cu and Ag–Ni). The parameters  $A$ ,  $\xi$ ,  $p$  and  $q$  for the homometallic interactions (Ag–Ag, Cu–Cu and Ni–Ni) are obtained by fitting to the experimental values of the cohesive energy, lattice parameters (by a constraint on the atomic volume), and independent elastic constants for the reference crystal structure at  $T = 0$  K.

For the heterometallic interactions (Ag–Cu and Ag–Ni), the parameters  $A$  and  $\xi$  are obtained by fitting to the solubility energy, and  $p$  and  $q$  are taken as the average of the pure ones. The potential parameters  $A$ ,  $\xi$ ,  $p$  and  $q$  for the pure metals (Ag, Cu, and Ni) and the Ag–Cu and Ag–Ni interactions were fitted by Ferrando and co-workers [23, 28, 30]. All the potential parameters were employed for the theoretical study of those bimetallic clusters with satisfactory results [23, 25, 28–32], and they are listed in table 1.

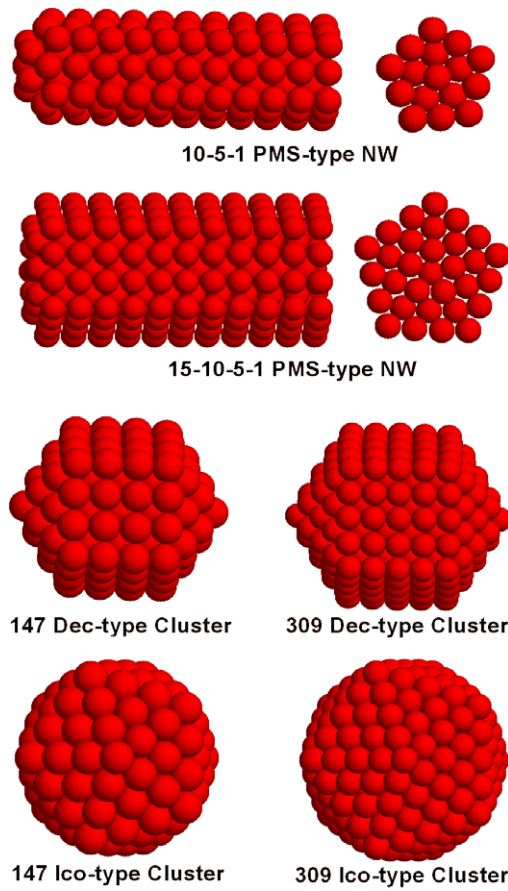


**Figure 1.** Morphologies of the initial shapes, including the 10–5–1 PMS-type NW, 15–10–5–1 PMS-type NW, 147-atom icosahedral (Ico-type) cluster, 309-atom icosahedral (Ico-type) cluster, 147-atom decahedral (Dec-type) cluster, and 309-atom decahedral (Dec-type) cluster.

**Table 1.** Parameters of the TB-SMA potential for the Ag–Cu and Ag–Ni bimetallic nanomaterials, including clusters and NWs. The parameters  $A$ ,  $\xi$ ,  $p$  and  $q$  for all the interactions are taken from Ferrando *et al* [28]. The parameter  $r_0$  is taken from Cleri and Rosato [43] for the pure metals (Ag, Cu and Ni), and taken as the average of the pure ones for the heterometallic interactions (Ag–Cu and Ag–Ni).

	$A$ (eV)	$\xi$ (eV)	$p$	$q$	$r_0$ (Å)
Ag–Ag	0.1031	1.1895	10.85	3.18	2.889
Cu–Cu	0.0894	1.2799	10.55	2.43	2.556
Ni–Ni	0.0958	1.5624	11.34	2.27	2.491
Ag–Cu	0.098	1.2274	10.700	2.805	2.723
Ag–Ni	0.096	1.3400	11.095	2.725	2.69

### 2.3. Monte Carlo method

In our study of the structural properties of the bimetallic clusters and NWs, semi-grand-canonical ensemble Monte Carlo (SEMI-GCMC) simulations were performed. In our study, periodic boundary conditions were applied along the NW axis, but no periodic boundary

conditions were used for the cluster. This method has been proved to be successful in the study of bimetallic alloys [44, 45], thin films [46], and clusters [27, 47–52]. Simulations and our programming details for the study of the structural properties of the bimetallic clusters can be found elsewhere in the literature [47, 48, 52] and in our previous work [27, 49–51].

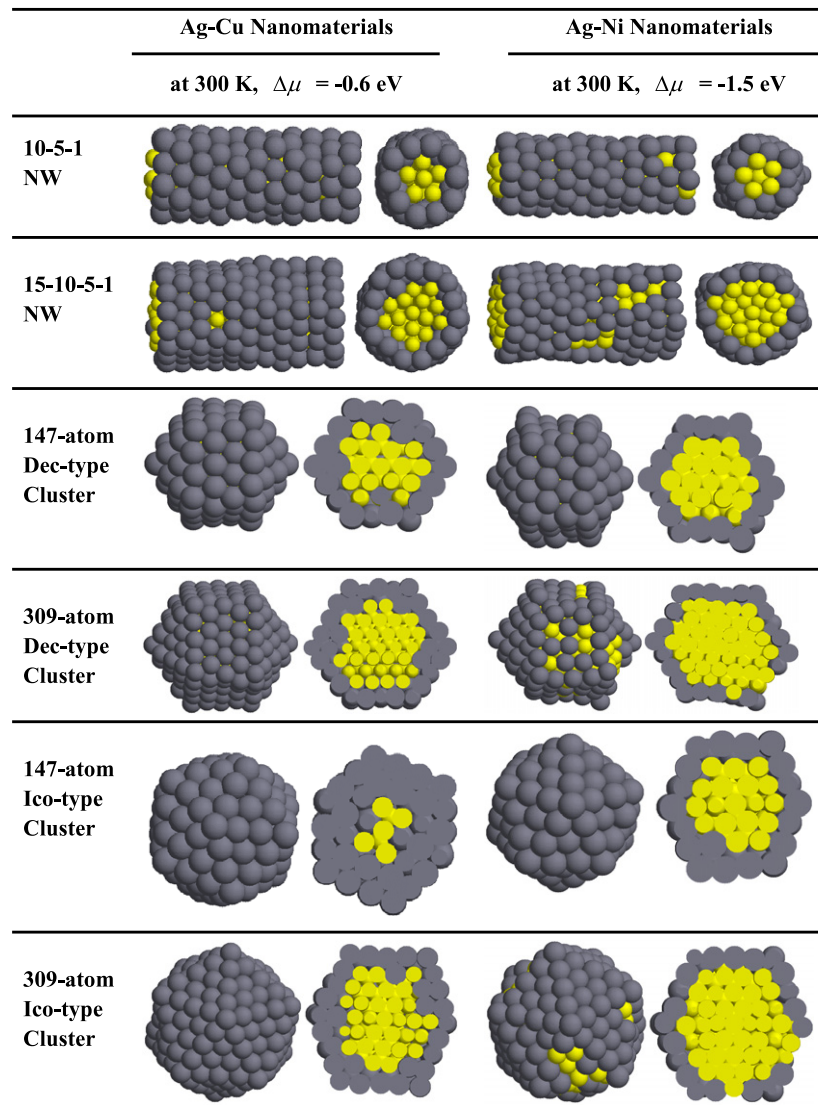
In our SEMI-GCMC simulation, the total number of atoms ( $N = N_{\text{Ag}} + N_{\text{M}}$ ,  $M = \text{Cu}$  or  $\text{Ni}$ ), temperature ( $T$ ) and chemical potential difference ( $\Delta\mu = \mu_{\text{Ag}} - \mu_{\text{M}}$ ,  $M = \text{Cu}$  or  $\text{Ni}$ ) between the two species were fixed. In the algorithm  $N_{\text{Ag}}$  and  $N_{\text{M}}$  ( $M = \text{Cu}$  or  $\text{Ni}$ ) were allowed to vary. The chemical composition at a given temperature was therefore obtained by performing the MC simulation at a fixed value of chemical potential difference  $\Delta\mu$  between the two species in the cluster. For the bimetallic cluster, the MC simulation method includes two types of trial. (1) A small displacement of a randomly selected atom from its original position in a random direction, which corresponds to the relaxation and vibration processes. The magnitude of the displacement was in the range  $(0, r_{\text{max}})$ . The maximum displacement  $r_{\text{max}}$  was dynamically adjusted in order to maintain the acceptance rate of new configurations close to 0.5. (2) Random selection of the chemical type of an atom, corresponding to the fixed chemical potential difference  $\Delta\mu$  between the two species and allowing the system to reach compositional equilibrium. The details of the simulation can also be found in our previous work [27, 49–51].

In this work, we chose the total length of the MC simulations to be 20000 steps for each atom. The first 10000 steps per atom were performed to achieve equilibrium under our criterion, in which the fluctuation of the total energy of the system was less than 0.2%, and the last 10000 steps per atom were used for an average of the structural properties of bimetallic clusters and NWs.

### 3. Results and discussion

Figure 2 shows the structures of four Ag–Cu and Ag–Ni nanomaterials, i.e. Ag–Cu bimetallic clusters and NWs, and Ag–Ni bimetallic clusters and NWs, at 300 K with  $\Delta\mu = -0.6$  and  $-1.5$  eV, respectively. It is found in figure 2 that the Ag–Cu and Ag–Ni bimetallic nanomaterials, including clusters and NWs, tend to form core–shell (CS) structures. It should be mentioned that CS structures were also found for Ag–Cu and Ag–Ni bimetallic clusters by using the genetic algorithm global optimization method [28]. However, only the small sizes of 34 and 38 atoms were focused on, due to large computational expenses of the global optimization method, compared with the method used in this work. In the CS structures, Ag atoms are enriched on the surface shell, while Cu or Ni atoms are in the core. The surface segregation phenomenon of Ag atoms in the Ag–Cu and Ag–Ni bimetallic clusters and NWs, forming the CS structure, is due to the lower surface energy of Ag ( $78 \text{ meV } \text{\AA}^{-2}$ ), compared with those for Cu ( $114 \text{ meV } \text{\AA}^{-2}$ ) and Ni ( $149 \text{ meV } \text{\AA}^{-2}$ ). In addition, the cohesive energy of Ag is 2.95 eV, while the cohesive energy of Cu and Ni is 3.49 and 4.44 eV, respectively. Thus, the Ag atom with the lower cohesive energy tends to occupy the surface to minimize the total energy. From figure 2, we can find that Ag–Cu and Ag–Ni nanomaterials, including clusters and NWs, possess the CS structure with different initial shapes, which implies that the initial shapes of the bimetallic clusters and NWs have little effect on the CS structure.

Cylindrical multi-shell-type (CMS-type) structures, which are composed by circular folding of the triangular network in a  $\langle 111 \rangle$  facet of fcc structure, are found in the Ag–Cu and Ag–Ni bimetallic 10–5–1 NWs at 300 K with  $\Delta\mu = -0.6$  and  $-1.5$ , respectively, as shown in figure 2. This means that the PMS-type structure with  $\langle 100 \rangle$ -like surfaces can be transformed into the CMS-type structure with  $\langle 111 \rangle$ -like surfaces at 300 K, which is in agreement with the

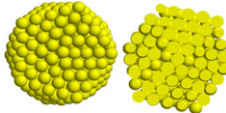
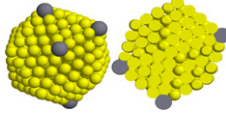
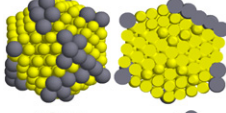
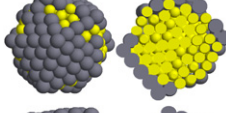
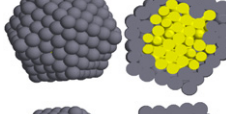
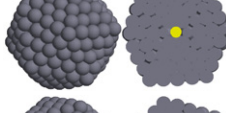
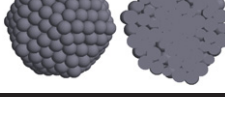


**Figure 2.** Morphologies of Ag–Cu and Ag–Ni nanomaterials with  $\Delta\mu = -0.6$  and  $-1.5$  eV, respectively, including the 10–5–1 NW, 15–10–5–1 NW, 147-atom icosahedral (Ico-type) cluster, 309-atom icosahedral (Ico-type) cluster, 147-atom decahedral (Dec-type) cluster, and 309-atom decahedral (Dec-type) cluster at 300 K (gray atoms, Ag; light atoms, Cu or Ni).

results for Cu NWs by Kang and Hwang [39]. Similar to the bimetallic 10–5–1 NWs, CMS-type structures are found for Ag–Cu and Ag–Ni bimetallic 15–10–5–1 NWs at 300 K with  $\Delta\mu = -0.6$  and  $-1.5$ , respectively, as shown in figure 2. Moreover, it is shown in figure 2 that some  $\langle 100 \rangle$  surfaces in the 147-atom and 309-atom Dec-type clusters are seldom found, and are transformed into  $\langle 111 \rangle$ -like surfaces at 300 K. However, the 147-atom and 309-atom Ico-type clusters retain their icosahedral shape with  $\langle 111 \rangle$ -like surfaces at 300 K. It is therefore concluded that the icosahedral shape is more stable than the decahedral shape for the 147-atom and 309-atom Ag–Cu and Ag–Ni bimetallic clusters at 300 K, while the CMS-type structure



**Table 2.** Compositions, total energies,  $\Delta - \Delta_{\min}$ , and morphologies of 309-atom Ag–Cu icosahedral clusters as a function of the chemical potential difference  $\Delta\mu$  ( $\Delta\mu = \mu_{\text{Ag}} - \mu_{\text{Cu}}$ ) at 300 K (gray atoms, Ag; light atoms, Cu).

Composition	$\Delta\mu$ (eV)	Total energy (eV)	$\Delta - \Delta_{\min}$ (eV)	Morphology
Ag <sub>0</sub> Cu <sub>309</sub>	−0.2	−1019.40	0.111 12	
Ag <sub>4</sub> Cu <sub>305</sub>	−0.3	−1018.09	0.092 454	
Ag <sub>30</sub> Cu <sub>279</sub>	−0.4	−1005.89	0.052 192	
Ag <sub>99</sub> Cu <sub>210</sub>	−0.5	−971.01	0	
Ag <sub>192</sub> Cu <sub>117</sub>	−0.6	−918.99	0.039 39	
Ag <sub>308</sub> Cu <sub>1</sub>	−0.7	−847.88	0.224 89	
Ag <sub>309</sub> Cu <sub>0</sub>	−1.1	−846.09	0.252 14	

is more stable than the PMS-type structure for the Ag–Cu and Ag–Ni bimetallic 10–5–1 and 15–10–5–1 NWs.

To monitor the effect of composition on the structure of Ag–Cu nanomaterials, we present the structures of 309-atom Ag–Cu icosahedral clusters at 300 K and different compositions. It should be mentioned that only core–shell structures with single-layer Ag shells and some fixed compositions can be obtained for Ag–Cu and Ag–Ni bimetallic clusters by using molecular dynamics simulations [23, 32]. Table 2 shows the compositions and morphologies of 309-atom Ag–Cu icosahedral clusters changing with the chemical potential difference  $\Delta\mu$  ( $\Delta\mu = \mu_{\text{Ag}} - \mu_{\text{Cu}}$ ) at 300 K. It is found in table 2 that the Ag mole fraction increases monotonically from 0% to 100% with the chemical potential difference  $\Delta\mu$  ranging from −0.2 to −1.1 eV for the seven different compositions, i.e., Cu<sub>309</sub>, Ag<sub>4</sub>Cu<sub>305</sub>, Ag<sub>30</sub>Cu<sub>279</sub>, Ag<sub>99</sub>Cu<sub>210</sub>, Ag<sub>192</sub>Cu<sub>117</sub>, Ag<sub>308</sub>Cu<sub>1</sub>, and Ag<sub>309</sub>. It is also found in table 2 that the Ag atoms are enriched on the surface shell covering the Cu atoms for 309-atom Ag–Cu icosahedral clusters, indicating the surface segregation of Ag atoms again. Also, with the increase of Ag mole fraction, the Ag atoms occupy the surface shell, interior shell, and central sites of 309-atom Ag–Cu icosahedral clusters in sequence at 300 K, as shown in table 2.



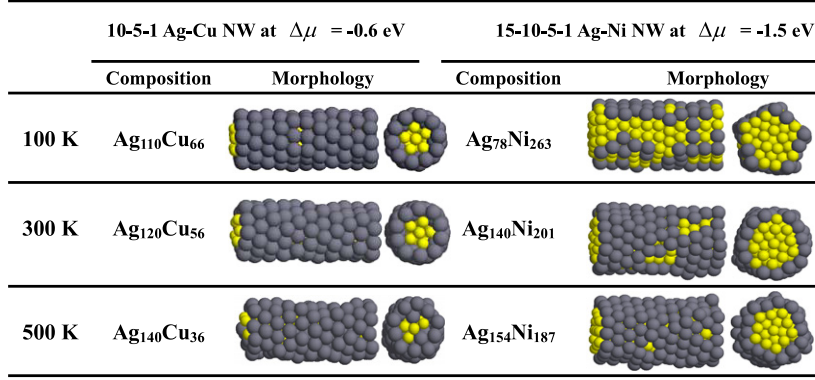


**Figure 3.** Morphologies of 10–5–1 Ag–Cu NWs and 15–10–5–1 Ag–Ni NWs with  $\Delta\mu = -0.6$  and  $-1.5$  eV, respectively, at 100, 300, and 500 K (gray atoms, Ag; light atoms, Cu or Ni).

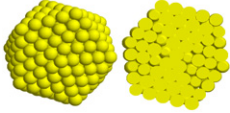
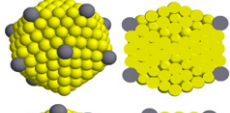
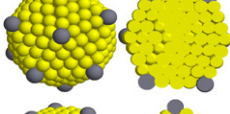
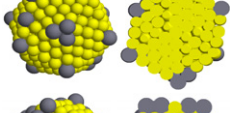
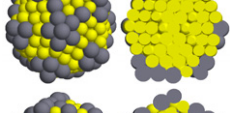
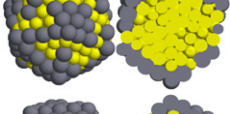
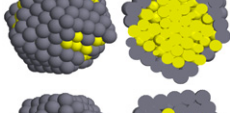
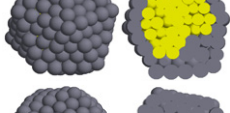
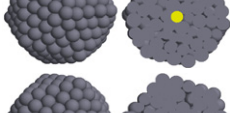
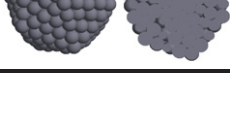
To compare the relative stability of bimetallic clusters with different compositions, a parameter,  $\Delta$ , is adopted for the bimetallic clusters, which is defined as the excess energy of the cluster with respect to  $N$  bulk atoms, divided by  $N^{2/3}$  [25, 28]:

$$\Delta = \frac{E_{\text{GM}}^{N_1, N_2} - N_1 \varepsilon_1^{\text{coh}} - N_2 \varepsilon_2^{\text{coh}}}{N^{2/3}} \quad (4)$$

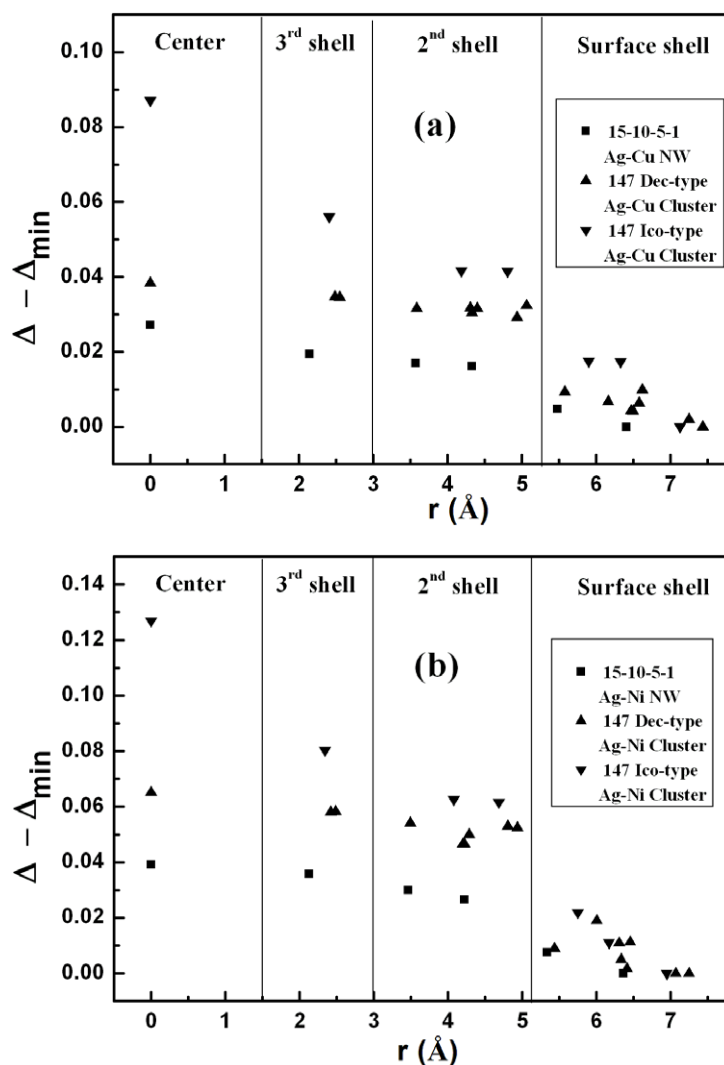
where  $N_1$  and  $\varepsilon_1^{\text{coh}}$  are the number and the bulk cohesive energy of the first chemical species, while  $N_2$  and  $\varepsilon_2^{\text{coh}}$  are the number and the bulk cohesive energy of the second one.  $N$  is the total number of atoms in the cluster with  $N = N_1 + N_2$ , and  $E_{\text{GM}}^{N_1, N_2}$  is the global minimum energy of the cluster at the given composition. Note that, the lower the  $\Delta$ , the more stable is the structure of the cluster. Table 2 shows the total energies and values of  $\Delta - \Delta_{\text{min}}$  for the 309-atom Ag–Cu icosahedral clusters with different compositions, where  $\Delta_{\text{min}}$  is the minimum value of  $\Delta$ . It is found in table 2 that the total energy increases with the increase of Ag mole fraction for the clusters, due to the different cohesive energies for the Ag and Cu. Also, our results reveal that the Ag<sub>99</sub>Cu<sub>210</sub> cluster has the lowest excess energy  $\Delta$ , as shown in table 2. Thus, we conclude that the most energetically favorable configuration measured by  $\Delta$  is the CS Ag<sub>99</sub>Cu<sub>210</sub> cluster for the 309-atom Ag–Cu icosahedral clusters at different compositions.

Table 3 shows the compositions, total energies, values of  $\Delta - \Delta_{\text{min}}$ , and morphologies of 309-atom Ag–Ni icosahedral clusters changing with the chemical potential difference  $\Delta\mu$  ( $\Delta\mu = \mu_{\text{Ag}} - \mu_{\text{Ni}}$ ) at 300 K. It is also found in table 3 that the Ag mole fraction increases monotonically with the chemical potential difference  $\Delta\mu$  ranging from  $-0.9$  to  $-1.9$  eV for ten different compositions, i.e., Ni<sub>309</sub>, Ag<sub>8</sub>Ni<sub>301</sub>, Ag<sub>10</sub>Ni<sub>299</sub>, Ag<sub>19</sub>Ni<sub>290</sub>, Ag<sub>53</sub>Ni<sub>256</sub>, Ag<sub>75</sub>Ni<sub>234</sub>, Ag<sub>123</sub>Ni<sub>186</sub>, Ag<sub>181</sub>Ni<sub>128</sub>, Ag<sub>308</sub>Ni<sub>1</sub>, and Ag<sub>309</sub>. Core–shell structures are also found for different compositions of 309-atom Ag–Ni icosahedral clusters at 300 K, where the Ag atoms are enriched on the surface shell, and the Ni atoms in the core (see table 3). In addition, it is found in table 3 that, with the increase of Ag mole fraction, the Ag atoms occupy the vertices of the surface shell, the edges of the surface shell, the interior shell, and the central sites of 309-atom Ag–Ni icosahedral clusters in sequence at 300 K. It is also found in table 3 that the total energy increases with the increase of Ag mole fraction for the clusters. Moreover, the energetic stability of the global minimum structures at different compositions is determined by the excess energy  $\Delta$ . From table 3, we can identify that the CS Ag<sub>123</sub>Ni<sub>186</sub> cluster is the most energetically favorable configuration for the 309-atom Ag–Ni icosahedral clusters at different compositions.

**Table 3.** Compositions, total energies,  $\Delta - \Delta_{\min}$ , and morphologies of 309-atom Ag–Ni icosahedral clusters as a function of the chemical potential difference  $\Delta\mu$  ( $\Delta\mu = \mu_{\text{Ag}} - \mu_{\text{Ni}}$ ) at 300 K (gray atoms, Ag; light atoms, Ni).

Composition	$\Delta\mu$ (eV)	Total energy (eV)	$\Delta - \Delta_{\min}$ (eV)	Morphology
Ag <sub>0</sub> Ni <sub>309</sub>	−0.9	−1307.13	0.290 25	
Ag <sub>8</sub> Ni <sub>301</sub>	−1.0	−1298.32	0.222 35	
Ag <sub>10</sub> Ni <sub>299</sub>	−1.1	−1296.55	0.195 82	
Ag <sub>19</sub> Ni <sub>290</sub>	−1.2	−1283.77	0.181 9	
Ag <sub>53</sub> Ni <sub>256</sub>	−1.3	−1239.36	0.045 19	
Ag <sub>75</sub> Ni <sub>234</sub>	−1.4	−1206.50	0.047 11	
Ag <sub>123</sub> Ni <sub>186</sub>	−1.5	−1137.13	0	
Ag <sub>181</sub> Ni <sub>128</sub>	−1.6	−1050.13	0.012 75	
Ag <sub>308</sub> Ni <sub>1</sub>	−1.7	−848.34	0.287 55	
Ag <sub>309</sub> Ni <sub>0</sub>	−1.9	−847.54	0.272 29	

Aiming at understanding the temperature effect on the structures of Ag–Cu and Ag–Ni nanomaterials, the morphologies of 10–5–1 Ag–Cu PMS-type NWs and 15–10–5–1 Ag–Ni PMS-type NWs with  $\Delta\mu = -0.6$  and  $-1.5$  eV, respectively, at 100, 300, and 500 K are shown in figure 3. As is seen in figure 3, CS structures are found for 10–5–1 Ag–Cu PMS-type NWs and 15–10–5–1 Ag–Ni PMS-type NWs at 100, 300, and 500 K, indicating that the CS structures of Ag–Cu and Ag–Ni NWs depend on temperature insignificantly. In addition, it is found in



**Figure 4.** The shift in excess energies  $\Delta - \Delta_{\min}$  (eV) of one impurity Ag in the Cu or Ni clusters and NWs as a function of  $r$  ( $\text{\AA}$ ), which is the distance of the Ag impurity from the geometrical center of the Cu or Ni clusters and NWs at 100 K. (a) A single impurity Ag in the 15–10–5–1 Cu PMS-type NW, 147-atom Cu decahedral (Dec-type) cluster, and 147-atom Cu icosahedral (Ico-type) cluster. (b) A single impurity Ag in the 15–10–5–1 Ni PMS-type NW, 147-atom Ni decahedral (Dec-type) cluster, and 147-atom Ni icosahedral (Ico-type) cluster.

figure 3 that the Ag–Cu and Ag–Ni NWs possess CMS-type structures at 100, 300, and 500 K. This means that the PMS-type structure with  $\langle 100 \rangle$ -like surfaces can be transformed into the CMS-type structure with  $\langle 111 \rangle$ -like surfaces for Ag–Cu and Ag–Ni bimetallic NWs even at 100 K, as shown in figure 3.

To understand the formation of the Ag–Cu and Ag–Ni CS structures, the excess energies  $\Delta$  of one impurity Ag in the Cu or Ni clusters and NWs of  $N$  atoms were calculated by using equation (4). In this work, we calculated the excess energies  $\Delta$  of a single impurity Ag placed in all the energetically inequivalent sites, which are 6, 17, and 7 for the 15–10–5–1 PMS-type NW, 147-atom decahedral cluster, and 147-atom icosahedral cluster, respectively. The shift

of the excess energies  $\Delta - \Delta_{\min}$  of the single impurity Ag in the 15–10–5–1 Cu PMS-type NW, 147-atom Cu decahedral cluster, and 147-atom Cu icosahedral cluster at 100 K, shown in figure 4(a), are obtained by shifting  $\Delta$  to the minimum value of  $\Delta$ . It is shown in figure 4(a) that the shift of the excess energies  $\Delta - \Delta_{\min}$  of the single impurity Ag in surface sites for the 15–10–5–1 Cu PMS-type NW, 147-atom decahedral Cu cluster, and 147-atom icosahedral Cu cluster are much lower than that of the cores, which means that the single Ag impurity prefers to stay on the surfaces of the clusters and NWs, rather than in the core sites for the Ag–Cu clusters and NWs. Similar results can also be found in figure 4(b) for Ag–Ni clusters and NWs, where the single Ag impurity lies on the surfaces of the Ni clusters and NWs, thus forming Ag–Ni core–shell bimetallic clusters and NWs. At the same time, as is measured by the shift of the excess energy  $\Delta - \Delta_{\min}$  of one impurity Ag in the Cu or Ni clusters, we can also find that the Ag atoms occupy the vertices of the surface shell, the edges of the surface shell, the interior shell, and the central sites of the clusters with the increase of Ag mole fraction in the Ag–Cu or Ag–Ni bimetallic clusters in sequence (see figures 4(a) and (b)).

#### 4. Conclusions

In summary, an effective Monte Carlo method was used to obtain the ground-state structures of Ag–Cu and Ag–Ni bimetallic nanomaterials, including clusters and nanowires (NWs), based on the second-moment approximation of the tight-binding potentials for the metal–metal interactions. The simulation results show that core–shell Ag–Cu and Ag–Ni structures can be obtained for the 10–5–1 pentagonal multi-shell-type (PMS-type) NWs, 15–10–5–1 PMS-type NWs, 147-atom icosahedral clusters, 309-atom icosahedral clusters, 147-atom decahedral clusters, and 309-atom decahedral clusters, in which Ag atoms generally lie on the surface, while Cu or Ni atoms prefer to occupy the core of the Ag–Cu or Ag–Ni bimetallic nanomaterials, including clusters and NWs. On the other hand, the Ag–Cu and Ag–Ni bimetallic NWs possess cylindrical multi-shell-type (CMS-type) structures at 100, 300, and 500 K, indicating that the PMS-type structure can be transformed into CMS-type structures for Ag–Cu or Ag–Ni NWs at 100, 300, and 500 K. Moreover, with the increase of Ag mole fraction in Ag–Cu or Ag–Ni bimetallic clusters, the Ag atoms occupy the surface shell, the interior shell, and the central sites of the clusters in sequence. Additionally, our studies show that the structures of Ag–Cu and Ag–Ni bimetallic clusters and NWs are insignificantly dependent on the initial shape, composition, and temperature. The excess energy  $\Delta$  of one impurity Ag in the Cu or Ni clusters and NWs was calculated to explain the formation of Ag–Cu and Ag–Ni core–shell bimetallic nanomaterials, including clusters and NWs. The single Ag impurity is favorable to being situated on the surfaces of the clusters and NWs, thus forming Ag–Cu and Ag–Ni core–shell bimetallic clusters and NWs.

#### Acknowledgments

This work is supported by the National Natural Science Foundation of China (Nos 20476004 and 20236010), and the National Basic Research Program of China (Grant No G2003CB615807).

#### References

- [1] Sinfelt J H 1983 *Bimetallic Catalysts: Discoveries, Concepts, and Applications* (New York: Wiley)
- [2] Toshima N and Yonezawa T 1998 *New J. Chem.* **22** 1179

- [3] Cottancin E, Lerme J, Gaudry M, Pellarin M, Vialle J L, Broyer M, Prevel B, Treilleux M and Melinon P 2000 *Phys. Rev. B* **62** 5179
- [4] Sun S, Murray C B, Weller D, Folks L and Moser A 2000 *Science* **287** 1989
- [5] Zitoun D, Amiens C, Chaudret B, Fromen M C, Lecante P, Casanove M J and Respaud M 2003 *J. Phys. Chem. B* **107** 6997
- [6] Scott R W J, Wilson O M, Oh S K, Kenik E A and Crooks R M 2004 *J. Am. Chem. Soc.* **126** 15583
- [7] Son S U, Jang Y, Park J, Na H B, Park H M, Yun H J, Lee J and Hyeon T 2004 *J. Am. Chem. Soc.* **126** 5026
- [8] Guzzi L 2005 *Catal. Today* **101** 53
- [9] Wang G F, Hove M A V, Ross P N and Baskes M I 2005 *Prog. Surf. Sci.* **79** 28
- [10] Walter E C, Murray B J, Favier F and Penner R M 2003 *Adv. Mater.* **15** 396
- [11] Choi W C and Woo S I 2003 *J. Power Sources* **124** 420
- [12] Darby S, Mortimer-Jones T V, Johnson R L and Roberts C 2002 *J. Chem. Phys.* **116** 1536
- [13] Baletto F and Ferrando R 2005 *Rev. Mod. Phys.* **77** 371
- [14] Toshima N, Harada M, Yonezawa T, Kushihashi K and Asakura K 1991 *J. Phys. Chem.* **95** 7448
- [15] Wang B L, Chen X S, Chen G B, Wang G H and Zhao J J 2004 *Solid State Commun.* **129** 25
- [16] Sankaranarayanan S K R S, Bhethanabotla V R and Joseph B 2006 *Phys. Rev. B* **74** 155441
- [17] Li H, Xu C L, Zhao G Y, Su Y K, Xu T and Li H L 2004 *Solid State Commun.* **132** 399
- [18] Su Y K, Qin D H, Zhang H L, Li H and Li H L 2004 *Chem. Phys. Lett.* **388** 406
- [19] Liu Q F, Wang J B, Yan Z J and Xue D S 2005 *Phys. Rev. B* **72** 144412
- [20] Mandal S, Selvakannan P R, Pasricha R and Sastry M 2003 *J. Am. Chem. Soc.* **125** 8440
- [21] Harpeness R and Gedanken A 2004 *Langmuir* **20** 3431
- [22] Toshima N, Kanemaru M, Shiraishi Y and Koga Y 2005 *J. Phys. Chem. B* **109** 16326
- [23] Baletto F, Mottet C and Ferrando R 2002 *Phys. Rev. B* **66** 155420
- [24] Wilson N T and Johnson R L 2002 *J. Mater. Chem.* **12** 2913
- [25] Rossi G, Rapallo A, Mottet C, Fortunelli A, Baletto F and Ferrando R 2004 *Phys. Rev. Lett.* **93** 105503
- [26] Hoof T V and Hou M 2005 *Phys. Rev. B* **72** 115434
- [27] Cheng D, Huang S and Wang W 2006 *Eur. Phys. J. D* **39** 41
- [28] Rapallo A, Rossi G, Ferrando R, Fortunelli A, Curley B C, Lloyd L D, Tarbuck G M and Johnson R L 2005 *J. Chem. Phys.* **122** 194308
- [29] Rossi G, Ferrando R, Rapallo A, Fortunelli A, Curley B C, Lloyd L D and Johnson R L 2005 *J. Chem. Phys.* **122** 194309
- [30] Baletto F, Mottet C and Ferrando R 2003 *Phys. Rev. Lett.* **90** 135504
- [31] Baletto F, Mottet C and Ferrando R 2003 *Eur. Phys. J. D* **24** 233
- [32] Baletto F, Mottet C, Rapallo A, Rossi G and Ferrando R 2004 *Surf. Sci.* **566–568** 192
- [33] Mariscal M M, Dassie S A and Leiva E P M 2005 *J. Chem. Phys.* **123** 184505
- [34] Gang L, Anderson B G, van Grondelle J, van Santen R A, van Gennip W J H, Niemantsverdriet J W, Kooyman P J, Knoester A and Brongersma H H 2002 *J. Catal.* **206** 60
- [35] Portales H, Saviot L, Duval E, Gaudry M, Cottancin E, Pellarin M, Lerme J and Broyer M 2002 *Phys. Rev. B* **65** 165422
- [36] Yang M, Wu C, Zhang C and He H 2004 *Catal. Today* **90** 263
- [37] Takahashi A, Hamakawa N, Nakamura I and Fujitani T 2005 *Appl. Catal. A* **294** 34
- [38] Kondo Y and Takayanagi K 2000 *Science* **289** 606
- [39] Kang J W and Hwang H J 2002 *J. Phys.: Condens. Matter* **14** 2629
- [40] Li H, Wang B L, Wang J L and Wang G H 2004 *J. Chem. Phys.* **121** 8990
- [41] Wang B L, Wang G H, Ren Y, Sun H Q, Chen X S and Zhao J J 2003 *J. Phys.: Condens. Matter* **15** 2327
- [42] Wang B L, Yin S Y, Wang G H and Zhao J J 2001 *J. Phys.: Condens. Matter* **13** L403
- [43] Cleri F and Rosato V 1993 *Phys. Rev. B* **48** 22
- [44] Foiles S M 1985 *Phys. Rev. B* **32** 7685
- [45] Foiles S M, Dowben P A and Miller A 1990 *Surface Segregation Phenomena* (Boca Raton, FL: CRC Press)
- [46] Hou M, Kharlamov V S and Zhurkin E E 2002 *Phys. Rev. B* **66** 195408
- [47] Zhurkin E E and Hou M 2000 *J. Phys.: Condens. Matter* **12** 6735
- [48] Hoof T V and Hou M 2004 *Appl. Surf. Sci.* **226** 94
- [49] Cheng D, Huang S and Wang W 2006 *Phys. Rev. B* **74** 064117
- [50] Cheng D, Huang S and Wang W 2006 *Chem. Phys.* **330** 423
- [51] Cheng D, Wang W and Huang S 2006 *J. Phys. Chem. B* **110** 16193
- [52] Zhurkin E E, Hautier G and Hou M 2006 *Phys. Rev. B* **73** 094108